Turkish Journal of Electrical Engineering & Computer Sciences

http://journals.tubitak.gov.tr/elektrik/

Research Article

Turk J Elec Eng & Comp Sci
(2016) 24: 2539 – 2555

doi:10.3906/elk-1403-30

Shunt active power filter control for compensating current power quality problems in three-phase three-wire systems based on an adaptive notch filter

Seyed Hossein TABATABAEI[1], **Mehran MOSLEHI BAJESTAN**[1], **Alireza JALILIAN**[2,*]
[1]Department of Electrical Engineering, Iran University of Science and Technology, Tehran, Iran
[2]Department of Electrical Engineering, Center of Excellence for Power System Automation and Operation, Iran University of Science and Technology, Tehran, Iran

Received: 04.03.2014 • **Accepted/Published Online:** 28.09.2014 • **Final Version:** 15.04.2016

Abstract: In this paper, a scheme is presented for properly compensating current power quality problems in a network. In this method, only by measuring grid current and using an adaptive notch filter (ANF), a reference sinusoidal current that is in phase with the grid voltage is created for the control system. Using ANFs guarantees the proper efficiency of the network when its frequency changes. A proportional controller and a resonance bank along with pulse width modulation are used in the shunt active power filter (SAPF) control system. One of the features of the resonant controller is its extremely high open-loop gain at its resonance frequency. This high gain causes the controller to accurately track the harmonic components. Simulations are carried out in MATLAB software under various conditions of load and network voltage, such as unbalanced and distortional voltage and changing load. These simulations verify the capabilities of this scheme.

Key words: Adaptive notch filter, indirect method, power quality, shunt active power filter

1. Introduction

Harmonic pollution and current unbalance in distribution networks caused by the expansion of nonlinear loads such as power electronic converters, computers, and fluorescent lights as well as the existence of single phase loads in three-phase networks are among the important issues in distribution networks, resulting in loss, overheating, and aging of equipment [1–3]. Passive filters, which have been used for a long time, and consist of inductors, capacitors, and resistors, are very simple, inexpensive, and fairly efficient. However, problems such as changes in frequency response with load variations, harmonics being compensated only one time by each filter, and so on have raised the subject of SAPFs [4].

In recent years, due to the reduction in costs of power electronic switches and digital signal processors, using active power filters has become more common. SAPFs are capable of improving the problems of grid current such as power factor correction, and compensating harmonic currents and unbalance. The schematic view of a typical SAPF and its connections is shown in Figure 1.

An SAPF is composed of a controller, a DC link capacitor, a coupling inductor, and a three-phase inverter. The most important part in an SAPF is its control system, which is divided into two parts; the first part generates the reference signal and the second part generates switching pulses. For the first part, various approaches have been presented in the literature by researchers. In [5], using instantaneous reactive power

*Correspondence: jalilian@iust.ac.ir

theory is proposed for calculating the reference compensating current that must be injected into the network. Since then, instantaneous reactive power theory has been used in many papers [6,7]. Using stationary reference frame, neural networks, time-domain current-detection algorithm, and sinusoidal integrator has been proposed in [8], [9], [4], and [10], respectively.

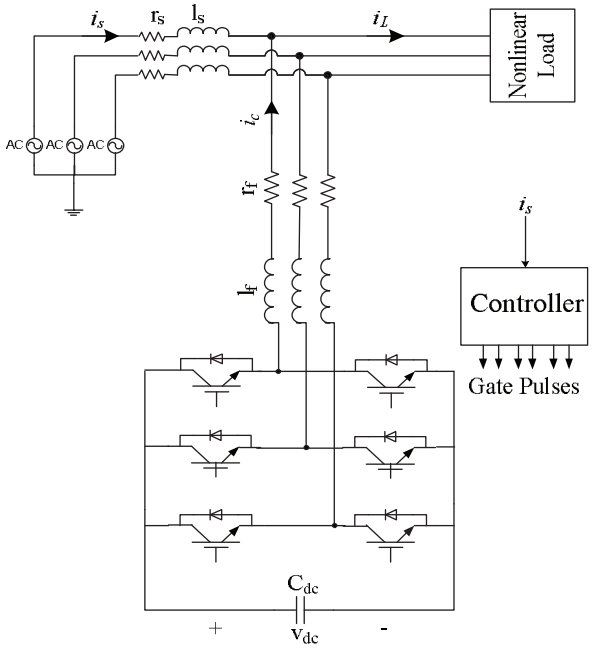

Figure 1. Configuration and connections of SAPF.

The part that generates switching signals is divided into two approaches: linear and nonlinear. The nonlinear approach or hysteresis current controller controls the current between two adjustable limits around the reference signal. The main drawback of this approach is its wide range of switching frequency that limits its applications. A controller such as a proportional-integral (PI) controller, a proportional-resonant (PR) controller, or a repetitive controller (RC) along with pulse width modulation is used in the linear approach [11].

Moreover, both direct and indirect methods are used to generate the current reference signal and control of the SAPF current. In the direct method, the load current and the output SAPF current are measured [12]. Among the disadvantages of this method is the need for a large number of sensors that causes increases delay and decreases dynamic response speed. However, in the indirect method, only the grid current is sampled. This causes a decrease in the number of sensors and thus increases dynamic response speed [13,14]. The disadvantage of this method is its inability to protect the over current in the power converter.

In this paper, a scheme is presented for compensating current power quality problems of the network including compensating reactive power, harmonics, and current unbalance due to negative sequence by a SAPF. To do this, the grid current is measured and its fundamental component is extracted by means of an ANF and a PI controller, which is responsible for regulating the voltage of DC link. Then this fundamental component is used for generating reference signals in the SAPF. These reference signals are tracked by an SAPF controller, which forces the converter to generate a waveform of current that is sinusoidal from the network's view.

The unique feature of the proposed control scheme is that there is no need to measure the grid voltage. During a period, the current reference signal will be in phase with the grid voltage. As a result of the reduction in sensors number, implementation of the SAPF is easier, its flexibility increases, and its cost falls.

Next, in the second section, the relationships and the structure of ANF are presented for extracting the components of load current. In the third section, it is explained how the reference current is generated by using the data of ANF and the DC link voltage controller. In the fourth section, considering the small signal model of SAPF, the control system of SAPF is designed by using a proportional-resonant (PR) controller and a DC link voltage controller. Simulation results and conclusions are presented in sections 5 and 6, respectively.

2. ANF for extracting the current components

In this section, a scheme based on ANF is presented for extracting current components. ANF has a basic structure for extracting sinusoidal components of a signal along with its frequency variations. Differential equations of this filter are expressed by Eqs. (1)–(3):

$$\ddot{x}_{ik} + i^2\theta^2 x_{ik} = 2\zeta_{ik}\theta e_k(t), i = 1, 2, \ldots, n; \quad k = \alpha, \beta \tag{1}$$

$$\dot{\theta} = -\gamma\theta \sum_{k=\alpha,\beta} x_k e_k(t) \tag{2}$$

$$e_k(t) = u_k(t) - \sum\nolimits_{l=1}^{n} \dot{\theta}_{lk}, \tag{3}$$

where θ is the frequency of the estimated fundamental component, and ζ_{ik} and γ are real adjustable positive values that determine the behavior of the ith subfilter in the system. These two parameters determine the steady state and transient behaviors of the filter, respectively. The input signal, $u(t) = \sum_{i=1}^{n} A_i \sin(\omega_i t + \varphi_i)$, has unknown values such as the nonzero amplitude A_i, ω_i frequencies and φ_i phases where $i = 1, 2...n$. The dynamic system expressed by Eqs. (1)–(3) has a unique periodic orbit located at [15]:

$$\begin{aligned} o &= \begin{pmatrix} o_1 \\ \vdots \\ o_n \\ \omega_0 \end{pmatrix} \\ o_i &= \begin{pmatrix} x_i \\ \dot{x}_i \end{pmatrix} = \begin{pmatrix} -\frac{A_i}{i\omega_0}\cos(i\omega_0 t + \varphi_i) \\ A_i \sin(i\omega_0 t + \varphi_i) \end{pmatrix} \end{aligned} \tag{4}$$

Eq. (4) shows that in each subfilter there are two outputs, one of which is equal to existing harmonic component in the input signal and the other one is equal to the derivative of that harmonic component. Using outputs given by Eq. (4), any kind of data about sinusoidal signals that comprise the input signal could be easily calculated. For example, the amplitude of harmonic voltage of ith order could be calculated using $A_i = \sqrt{(i\omega_0)^2 x_i^2 + \dot{x}_i^2}$ in the outputs of the ith subfilter. In fact, ANF is a sinusoidal signal integrator filter that corrects its own resonance frequency by measuring the network frequency. The detail of the structure of the ANF used in this paper is shown in Figure 2.

In this figure, i_{nx} and $S_{90}i_{nx}$ represent the input signal's harmonic component of nth order and its derivative, respectively.

In a three-phase system, three ANFs are required [15]. However, by the use of the $\alpha\beta$ transform, the current could be changed from three-phase to two-phase and, as a result, one of the filters could be removed. The $\alpha\beta$ transform can be calculated using the following equations:

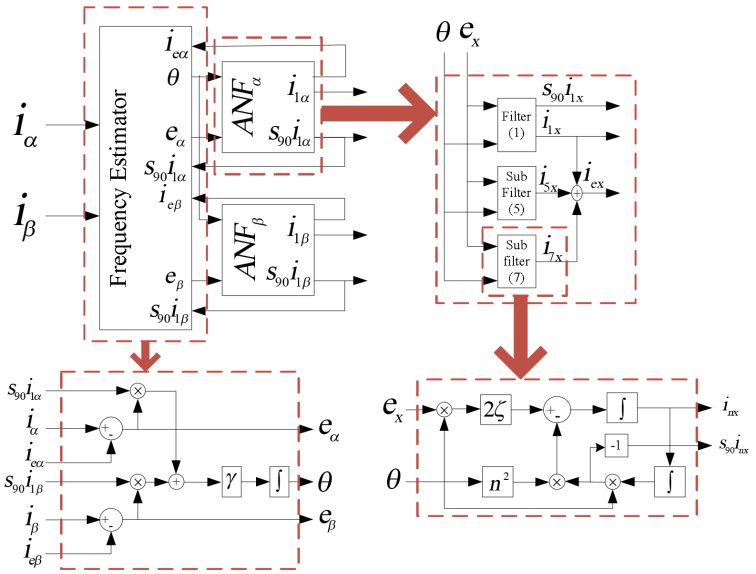

Figure 2. Structure of the ANF used in this paper.

$$\begin{bmatrix} i_\alpha \\ i_\beta \end{bmatrix} = \sqrt{\frac{2}{3}} \begin{bmatrix} 1 & -\frac{1}{2} & -\frac{1}{2} \\ 0 & \frac{\sqrt{3}}{2} & -\frac{\sqrt{3}}{2} \end{bmatrix} \begin{bmatrix} i_a \\ i_b \\ i_c \end{bmatrix} \tag{5a}$$

and

$$\begin{bmatrix} i_a \\ i_b \\ i_c \end{bmatrix} = \sqrt{\frac{2}{3}} \begin{bmatrix} 1 & 0 \\ -\frac{1}{2} & \frac{\sqrt{3}}{2} \\ -\frac{1}{2} & -\frac{\sqrt{3}}{2} \end{bmatrix} \begin{bmatrix} i_\alpha \\ i_\beta \end{bmatrix}. \tag{5b}$$

Here the ANF is composed of a filter for fundamental component, and two subfilters for the harmonic components of 5 and 7 orders. Using this combination decreases the error of frequency estimation and the errors of outputs of main filter and subfilters with a very high accuracy. It should be mentioned that the initial values of all integrators are zero except for the integrator of frequency estimation part. This integrator is set to the nominal frequency of the networks [15]. For more information regarding the ANF, refer to [16].

In addition, for the sake of more simplification, if currents of all three phases are similar except for a difference of 120 degrees between each two phases, first the components comprising the current in phase 'a' are extracted then by using unit template vector, the components of other two phases could be calculated virtually [17].

3. Generating reference current signal

In this paper, the indirect method is used to control the network current. In the direct method, the controller uses the load current and output current of SAPF, but in the indirect method just the source current is sampled and this decreases the costs and increases the speed of dynamic response.

In this method, a sinusoidal signal is generated as the reference signal and the SAPF is responsible for generating a waveform of current that makes the grid current closer to the reference current. Therefore, generating the reference current of source is one of the important control parts of the SAPF.

As can be seen in Figure 3, once the current of each phase is measured, it is transferred to the $\alpha\beta$ frame. The ANF is responsible for extracting the fundamental component of current in $\alpha\beta$ axes. Once the fundamental current component and its derivative are separated by the ANF, the inverse $\alpha\beta$ transform is taken of these outputs. Now, the fundamental components of current of each phase and their derivatives are available. In order to compensate the unbalance of grid current, the average values of the currents of fundamental component are calculated. Now, the reference current of the grid could be calculated by multiplying the following three factors:

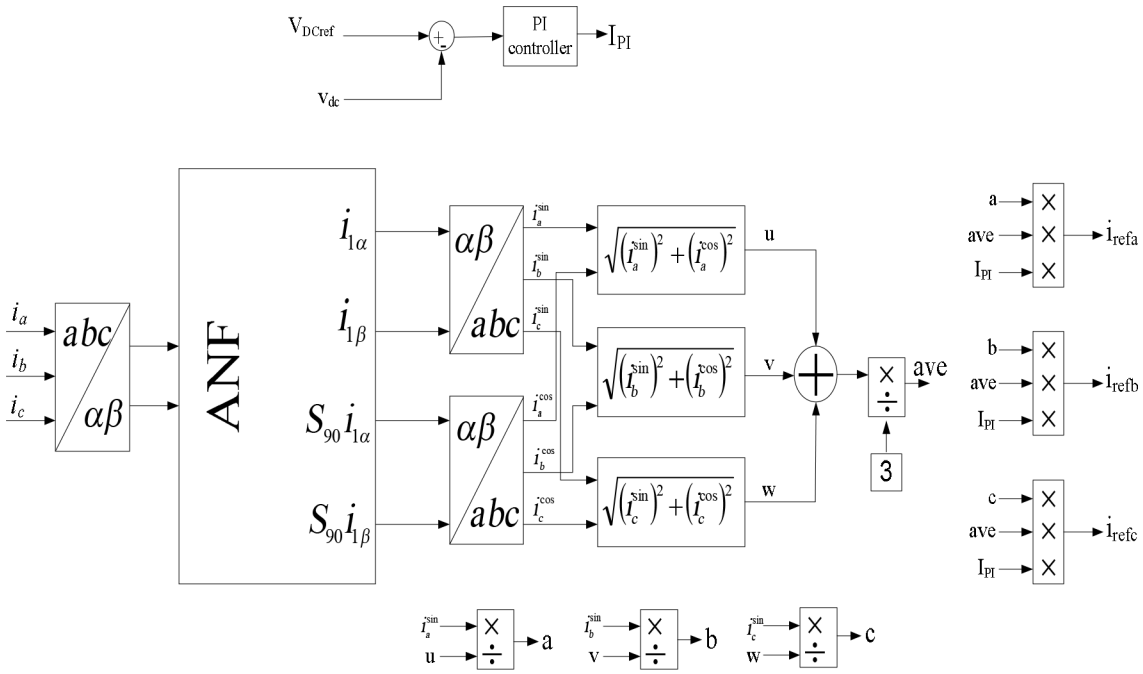

Figure 3. The way the reference current is generated in the proposed scheme.

1) The output of PI controller, which is responsible for regulating DC link voltage.

2) The average values of currents of three phases of the network.

3) The fundamental component of current of each phase with amplitude of unity.

In section 4.3, it is explained that how reactive power is compensated.

4. Designing the control system

SAPF control is composed of two interconnected loops: 1) inner control loop, which is responsible for matching the grid current with the reference current, 2) outer control loop, which adjusts the DC link voltage at the desirable value. To avoid the interference of these two control loops, the inner control loop is designed in a way that it is faster than the outer loop as much as possible [18].

4.1. Designing the inner loop

To design the inner control loop, the small signal model of the SAPF with its controller is shown in Figure 4.

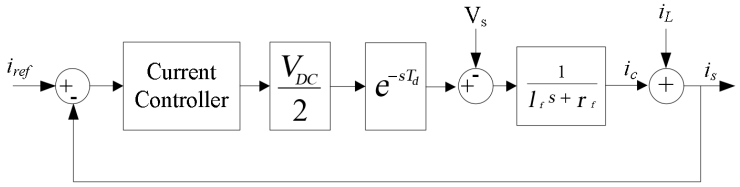

Figure 4. The block diagram of current control loop.

In the design of the current controller, regardless of type of application, the error between the reference current and the real current is used for adjusting switching signals of the power electronic converter. The objectives of current controller are generally as follows [11]:

- Achieving minimum amplitude and phase errors and finally achieving the desirable error value of zero,
- Accurately tracking the reference current signal in transient time, which means a frequency response that is as large as possible,
- Limiting the current peak in order to prevent overloading.

Considering the aforementioned points, PI controllers could be used in control systems with rotating frame and PR controllers could be used in control systems with stationary frame. Since the stationary frame is used in this paper, the transfer function of the PR current controller is considered as the following equation:

$$G_c(s) = k_p + \sum_{i=1,5,7,11,13} \frac{2k_i\omega_r s}{s^2 + 2\omega_r s + (i\omega_n)^2}, \tag{6}$$

where k_p is the proportional gain, k_i is the resonant gain, ω_n denotes the nominal frequency of the network, and ω_r is the cut-off frequency. Harmonics of the orders of up to 13 are considered as the dominant current harmonics. As can be seen in Figure 4, the grid current (i_s) depends on three factors: the reference current, grid voltage, and load current. The grid current could be written as Eq. (7):

$$i_s = G_1 i_{ref} + G_2 V_s + G_3 i_L \tag{7}$$

$$G_1 = \frac{G_c V_{DC}}{G_c V_{DC} + 2r_f e^{sT_d} + 2l_f s e^{sT_d}}$$

$$G_2 = \frac{-2e^{sT_d}}{G_c V_{DC} + 2r_f e^{sT_d} + 2l_f s e^{sT_d}}$$

$$G_3 = \frac{2e^{sT_d}(l_f s + r_f)}{G_c V_{DC} + 2r_f e^{sT_d} + 2l_f s e^{sT_d}}$$

where G_C is the current controller, T_d represents the delays caused by sampling and pulse width modulation, $V_{DC}/2$ is the converter gain, and l_f and r_f are the inductance and the coupling resistor between the converter and the grid, respectively. To have a grid current that is less affected by the load current and grid voltage, the coefficients of controller, G_C, need to be as large as possible. However, existence of delays in the equations causes the selected ranges for the control coefficients to be small. According to [11], it could be assumed that $T_d = 0.75/f_{sw}$, where, f_{sw} is the switching frequency of the converter. The goal is to determine the values

of control gains of G_C, so that phase margin and gain margin of open loop transfer function are in a certain range. According to [19], the desirable phase margin is considered to be between 30 and 60 degrees and gain margin is considered to be greater than 6 dB. Considering

$$G_{inv} = \frac{V_{DC}}{2} e^{-T_d s} \frac{1}{l_f s + r_f}$$

The phase and gain margins, which are constraints for determining control coefficients, are determined by Eq. (8):

$$\angle \{G_c(j\omega_c) G_{inv}(j\omega_c)\} = -\pi + \varphi_m \tag{8a}$$

$$k_a = -20 \log |G_c(j\omega_a) G_{inv}(j\omega_a)| \tag{8b}$$

where φ_m is the phase margin, ω_c is the gain crossover frequency, k_a is the gain margin, and ω_a is the phase crossover frequency [19]. To determine the control coefficients, the phase margin is calculated:

$$\angle \{G_c(j\omega_c) G_{inv}(j\omega_c)\} = \angle \left\{ \left(k_p + \sum_{i=1,5,7,11,13} \frac{j2k_i\omega_r\omega_c}{-\omega_c^2 + j2\omega_r\omega_c + (i\omega_n)^2} \right) \left(\frac{V_{DC}}{2} \frac{e^{-jT_d\omega_c}}{jl_f\omega_c + r_f} \right) \right\}$$

Assuming that $i\omega_n \ll \omega_c$:

$$\angle \frac{V_{DC}}{2} \left(k_p + \frac{j2\omega_r\omega_c \left(\sum_i k_i \right)}{-\omega_c^2 + j2\omega_r\omega_c} \right) \left(\frac{e^{-jT_d\omega_c}}{jl_f\omega_c + r_f} \right)$$

Consequently,

$$\tan^{-1} \frac{k_p\omega_c}{2\omega_r \left(k_p + \sum_i k_i \right)} - T_d\omega_c - \tan^{-1} \frac{\omega_c}{2\omega_r} - \tan^{-1} \frac{l_f\omega_c}{r_f} = -\pi + \varphi_m \tag{9}$$

Since ω_c is large, Eq. (9) could be rewritten as follows:

$$\frac{\pi}{2} - \omega_c T_d - \frac{\pi}{2} - \frac{\pi}{2} = -\pi + \varphi_m$$

Therefore, assuming an appropriate phase margin, the gain crossover frequency could be calculated using Eq. (10):

$$\omega_c = \frac{\pi/2 - \varphi_m}{T_d} \tag{10}$$

Since the magnitude of open loop transfer function, $G_C(s) G_{inv}(s)$, is equal to unity at the gain crossover frequency, the following equation could be written:

$$1 = \frac{V_{DC}}{2} \frac{\sqrt{k_p^2\omega_c^4 + 4\omega_r^2\omega_c^2 \left(k_p + \sum_i k_i \right)^2}}{\sqrt{4\omega_r^2\omega_c^2 + \omega_c^4}} \frac{1}{\sqrt{\omega_c^2 l_f^2 + r_f^2}}$$

where k_p could be approximated using Eq. (11):

$$k_p \approx \frac{2\omega_c l_f}{V_{DC}} \tag{11}$$

In (9), we supposed that $\tan^{-1}\frac{k_p\omega_c}{2\omega_r\left(k_p+\sum\limits_i k_i\right)}$ is approximately equal to 90 degrees (or its exact value, 87 degrees, could be considered). The same equation is used to determine k_i:

$$\frac{k_p\omega_c}{2\omega_r\left(k_p+\sum\limits_i k_i\right)} = 20 \tag{12}$$

If it is assumed that all k_is are equal, we obtain

$$\frac{k_p\omega_c}{2\omega_r\left(k_p+5k_i\right)} = 20$$

And as a result

$$k_i = \frac{k_p\left(\omega_c - 40\omega_r\right)}{200\omega_r} \approx \frac{k_p\omega_c}{200\omega_r} \tag{13}$$

Figure 5 shows the open loop frequency response of the system, which is obtained by using the data in Table 1. The frequency responses of transfer functions G1, G2, and G3 are shown in Figure 6. As can be seen in this figure, these frequency responses have properly tracked the reference current system and there is no tracking error in the fundamental grid frequency and harmonics. However, due to the small proportional coefficient k_p, this error exists in other frequencies. Moreover, the effect of load current harmonics and grid voltage on the grid current could be ignored.

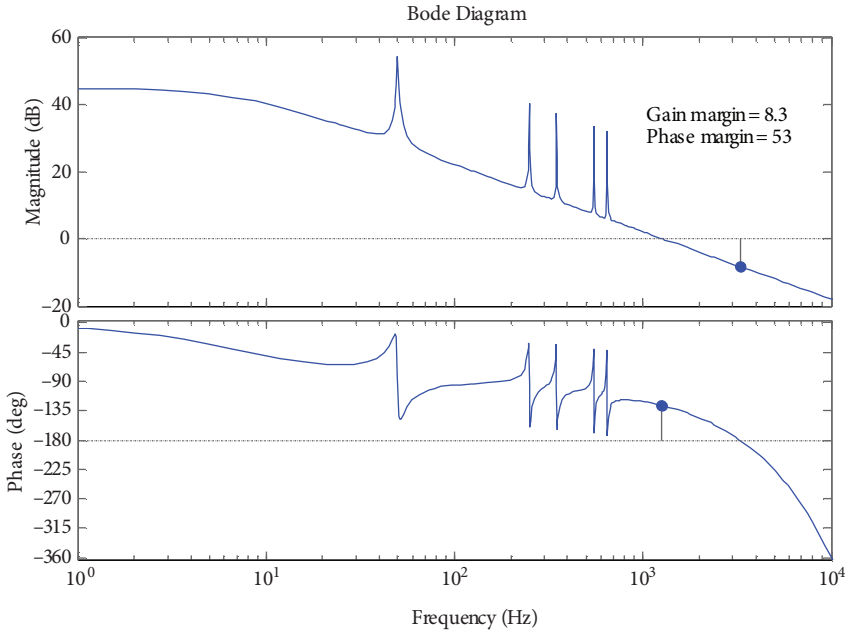

Figure 5. The open loop frequency response of the system shown in Figure 4.

Table 1. Parameters used in simulations.

Parameter	Value
Line-to-line voltage of the grid	380 V
Grid frequency	50 Hz
Grid inductance, l_s	0.1 mH
Resistance of diode nonlinear load	10 Ω
Inductance of diode nonlinear load	0.1 H
Parameters of the ANF	$\gamma = 8000$ $\zeta_1 = 0.5$ $\zeta_{7.5} = 0.3$
DC link voltage	700 V
The capacitance of DC link	2200 μF
The output inductance of filter, l_f	2.2 mH
The output resistance of filter, r_f	0.1 Ω
Switching frequency	10 kHz
Current controller (PR)	$K_p = 0.05$ $K_i = 0.74$ $\omega_r = 2$
PI controller of outer loop	$K_p = 1.45$ $K_i = 60$

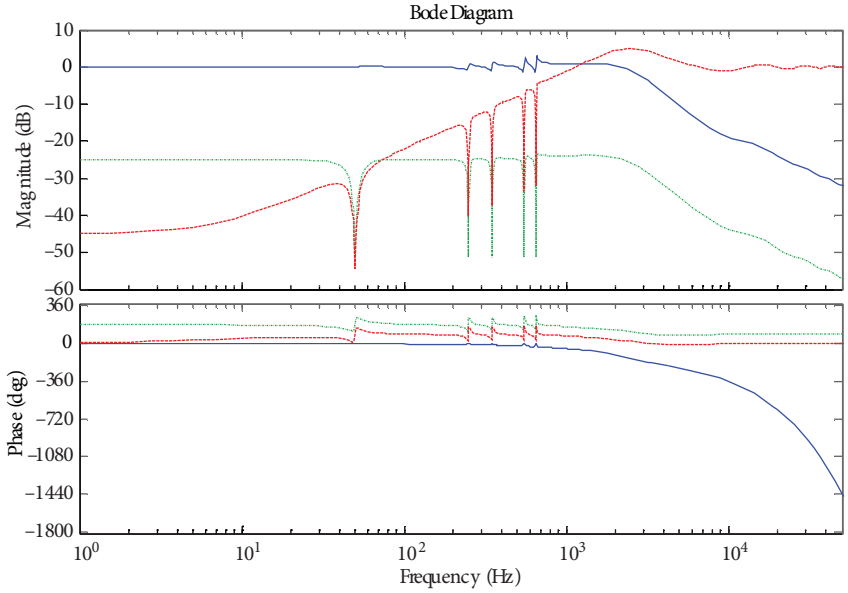

Figure 6. Frequency responses of G1 (blue), G2 (green), and G3(red).

4.2. Designing the outer loop

The outer control loop is responsible for keeping the DC link voltage at a fixed value. Regulating the DC link voltage requires absorbing active power from the grid by the SAPF, and a PI controller is generally used in this part. To obtain the equations that govern this part, the following equation could be written based on the

power balance equations in the grid [20]:

$$p_{dc} = \frac{d}{dt}\left(\frac{1}{2}C_{DC}v_{dc}^2\right) = C_{DC}v_{dc}\frac{dv_{dc}}{dt} \tag{14}$$

where p_{dc} is the power required for regulating the DC link voltage. Furthermore,

$$p_{ac} = \sum_{i=a,b,c} v_i i_{ci} - \sum_{i=a,b,c} r_f i_{ci}^2 - \sum_{i=a,b,c} \frac{d}{dt}\left(\frac{1}{2}l_f i_{ci}^2\right) \tag{15}$$

In a balanced three-phase system,

$$C_{DC}v_{dc}\frac{dv_{dc}}{dt} = 3v_s i_c - 3r_f i_c^2 - 3l_f i_c \frac{di_c}{dt} \tag{16}$$

By applying a small perturbation disturbance around the operating point at v_{dc} and i_c, also by linearization Eq. (16) around the operating point and ignoring terms of higher orders, the following equation is obtained:

$$\begin{cases} v_{dc} = V_{DC} + \Delta v_{dc} \\ i_c = I_c + \Delta i_c \end{cases}$$
$$3v_s I_c + 3v_s \Delta i_c - 3r_f I_c^2 - 6r_f I_c \Delta i_c - 3l_f I_c \frac{d\Delta i_c}{dt} = V_{DC}C_{DC}\frac{d\Delta v_{dc}}{dt} \tag{17}$$

where, in steady state, $3v_s I_c - 3r_f I_c^2 = 0$.

Taking the Laplace transform on Eq. (17) determines the transfer function of DC link voltage variation to SAPF output current variations:

$$\frac{\Delta v_{dc}}{\Delta i_c} = G_{DC}(s) = \frac{-3l_f I_c s + 3v_s - 6r_f I_c}{C_{DC}V_{DC}s} \tag{18}$$

In the equation above, I_c, v_s, and V_{DC} are the effective values of the operating point. If a PI controller is used for regulating the DC link voltage, the block diagram of the closed loop control system will be as shown in Figure 7. Adjusting the coefficients of the PI controller is simply carried out by considering a maximum overshoot value of 10%. The calculated parameters are shown in Table 1, and Figure 8 shows the open loop frequency response diagram of the system shown in Figure 7.

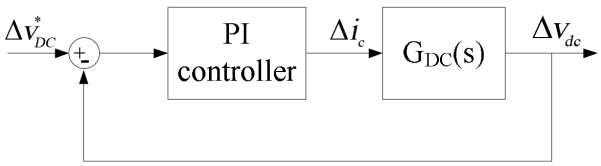

Figure 7. The block diagram of DC link voltage control system.

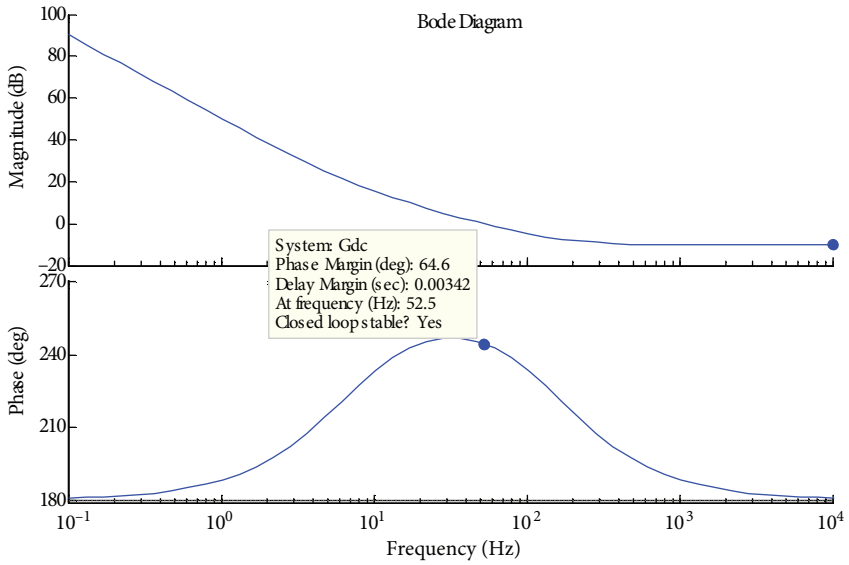

Figure 8. The open loop frequency response of DC link voltage control system.

4.3. Reactive power compensation

Let us assume that the load only includes active and reactive power components at the fundamental frequency. Furthermore, it is assumed that the loss of active shunt filter is very low and ignorable. From Figure 1, it can be concluded that

$$i_s + i_c = i_L \tag{19}$$

Moreover, from Figure 4, it is clear that i_c is equal to

$$i_c = (i_{ref} - i_s)\, G_c\,(j\omega_n)\, G_{inv}\,(j\omega_n) \tag{20}$$

On the other hand, considering the way the reference current is generated in Figure 3, $i_{ref} = ki_s$, where, in steady state, k is a fixed number and is equal to the output of PI controller. Therefore, the following equation could be written:

$$i_c = (ki_s - i_s)\, G_c\,(s)\, G_{inv}\,(s) = i_s\,(k-1)\, G_c\,(s)\, G_{inv}\,(s) \tag{21}$$

Since it is assumed that the load current is only composed of fundamental component, behavior of the controller, G_c, at fundamental frequency could be considered as the following equation:

$$G_c\,(s) = k_p + \frac{2k_1\omega_r s}{s^2 + 2\omega_r s + \omega_n^2} \tag{22}$$

Using Eqs. (19), (21), and (22), the control system shown in Figure 9 at the frequency of fundamental component is obtained.

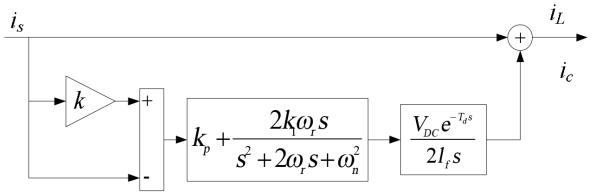

Figure 9. The control block diagram of SAPF at fundamental frequency and in a lossless condition.

Now we consider the system at the steady state; since the SAPF does not have any source of energy, it cannot generate active power. Therefore, the active power required by the load is supplied by the network. On the other hand, the reactive power in a lossless system does not need any source of energy [21]. Therefore, if the control system is designed properly, the SAPF is capable of supplying the reactive power. The reactive power of the load is considered as

$$i_{L_q}(t) = a \times sin(\omega_n t) \tag{23}$$

where i_{L_q} is the reactive component of the load current and has a certain value. Considering Figure 9, the reactive component of the load current is equal to

$$i_{L_q}(s) = i_{s_q}(s) + \left(k i_{s_q}(s) - i_{s_q}(s)\right)\left[\left(k_p + \frac{2k_1\omega_r s}{s^2 + 2\omega_r s + \omega_n^2}\right)\left(\frac{V_{DC}e^{-T_d s}}{2l_f s}\right)\right]$$

Thus, the reactive component of the grid current is equal to

$$i_{s_q}(s) = \frac{i_{L_q}(s)}{1 + (k-1)\left[\left(k_p + \frac{2k_1\omega_r s}{s^2+2\omega_r s+\omega_n^2}\right)\left(\frac{V_{DC}e^{-T_d s}}{2l_f s}\right)\right]} \tag{24}$$

Using the final value theorem of the Laplace transform (Eq. (25)), the final value of the reactive current of the network could be calculated:

$$f(t) = sF(s) \tag{25}$$

$$si_{s_q}(s) = \frac{s\frac{a\omega}{s^2+\omega^2}}{1 + (k-1)\left[\left(k_p + \frac{2k_1\omega_r s}{s^2+2\omega_r s+\omega_n^2}\right)\left(\frac{V_{DC}e^{-T_d s}}{2l_f s}\right)\right]} = 0 \tag{26}$$

Eq. (26) shows that, under steady state conditions, the load reactive current is not supplied by the network.

5. Simulation results

This section presents the results of simulations that are carried out in MATLAB environment. Compensating harmonic current, unbalance, and reactive component of the network are carried out under various conditions. Five different cases of load and network voltage are considered in simulations. These cases will be investigated in this section. Parameters used in simulations are shown in Table 1.

In addition, the simulation results of the proposed control scheme have been compared with the results of the control scheme shown in Figure 10. This comparison is presented in Table 2.

a) The first case involves compensating grid current when a diode rectifier is connected to the network as a nonlinear load.

   Simulation results are shown in Figure 11, while harmonic spectrums of load and grid currents after compensation are shown in Figure 12. In this case, the grid voltage is considered to be symmetric and sinusoidal, and load current THD is decreased from 23.6% to 3.2% in grid current.

b) The second case is analyzed in order to investigate the dynamic behavior of SAPF. At t = 0.35 s, nonlinear load of the network has been increased by a factor of 50%. Simulation results are shown in Figure 13.

Table 2. The comparison of simulation results of the proposed control scheme with conventional control scheme.

	Proposed Scheme		Conventional scheme
Case A	phase	THD (%)	
	A	3.21	3.6
	B	3.42	2.77
	C	3.1	3.78
Case B	DC link voltage undershoot/overshoot (%)		
	5.7/5		8.3/3
Case C	Phase	THD (%)	
	A	3.65	3.87
	B	3.95	4.55
	C	4.33	4.80
Case D	Average of source current (rms) (A)		
	46.1		46

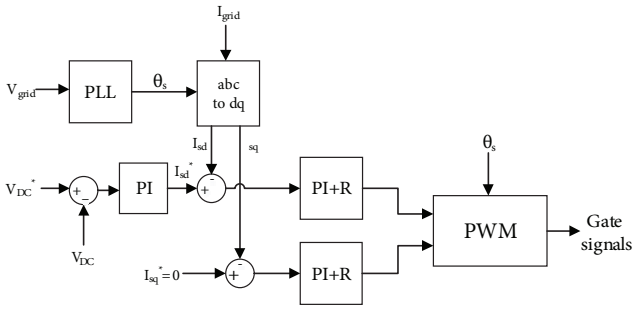

Figure 10. Diagram of a conventional control schemes.

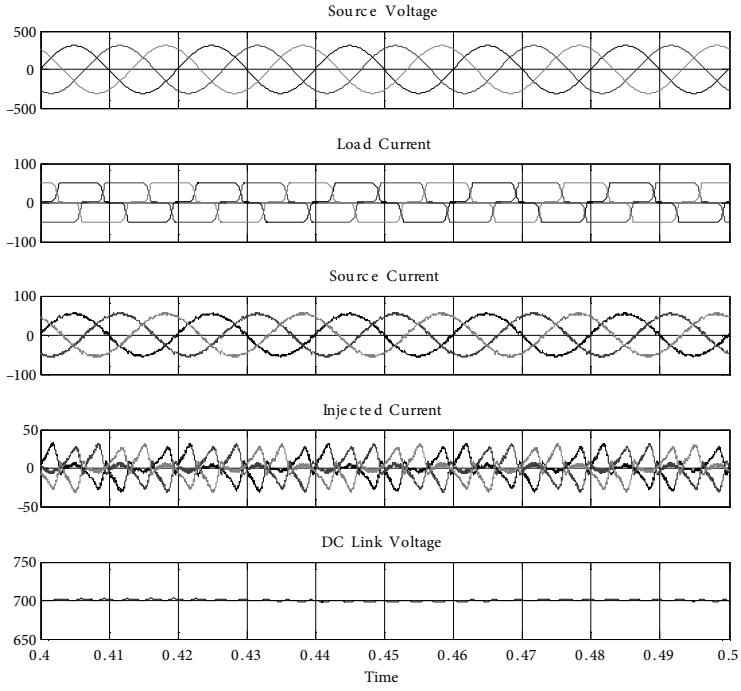

Figure 11. Simulation results of the first case, for compensating grid current harmonics.

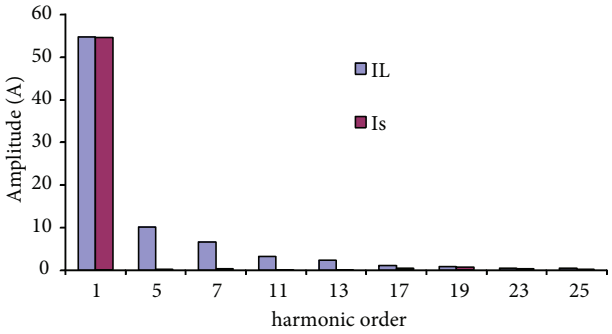

Figure 12. Harmonic spectrums of load and grid currents after compensation.

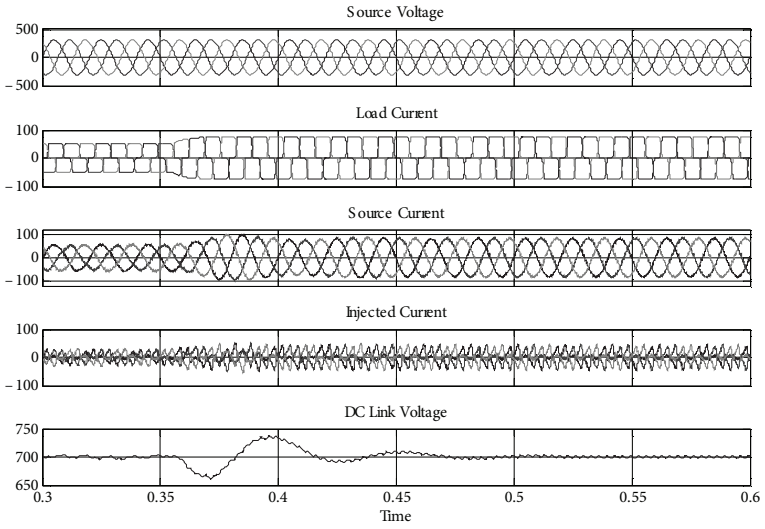

Figure 13. Simulation results of the second case for investigating the dynamic response of the SAPF to load variations.

As can be seen in Figure 13, the grid current at the moment of load increase has tracked the reference current with a small overshoot, and the DC link voltage is well restored, which indicates the proper dynamic behavior of the control system.

c) In the third case, the effect of voltage harmonics and unbalance on the performance of SAPF is investigated. Figure 14 shows the simulation results of this case. In this simulation, a 5% unbalance is added to fundamental component and harmonic of fifth order with amplitude of 0.1 pu is added to nominal voltage of the system. As it was shown in the frequency response of transfer function G2 in sections 1–4, voltage harmonics have an insignificant effect on the performance of the SAPF control system. The harmonic spectrum of load current (THD = 23.5%) and grid current (THD = 3.65%) in phase 'a' after simulation is shown in Figure 15.

d) In the fourth case, simulation results show the performance of SAPF in balancing the grid current. In this case, a linear load is placed between phases 'a'and 'c' in order to make the load current unbalanced. Figure 16 shows the simulation results of this case. As can be seen in this figure, the proposed control scheme is highly capable of balancing load current. Data of each phase are presented in Table 3.

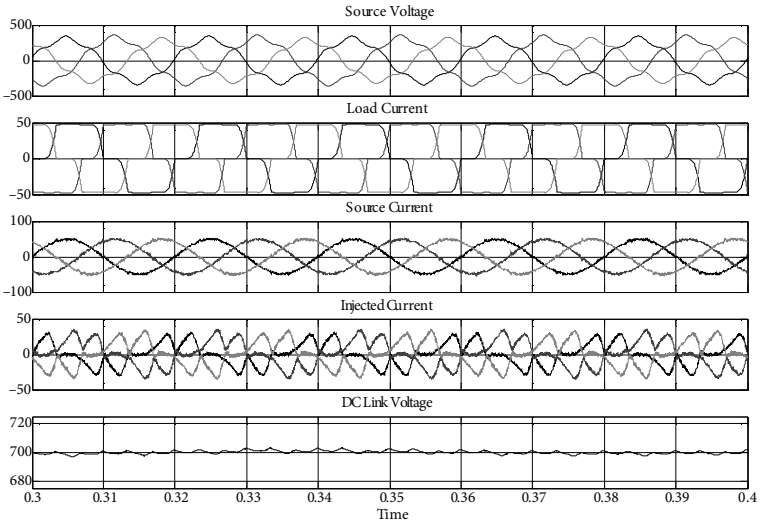

Figure 14. simulation results of the third case under the conditions of harmonic and unbalanced grid voltage.

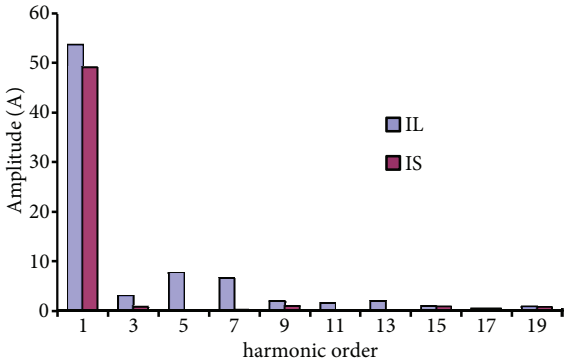

Figure 15. Harmonic spectrums of load and grid currents after compensation.

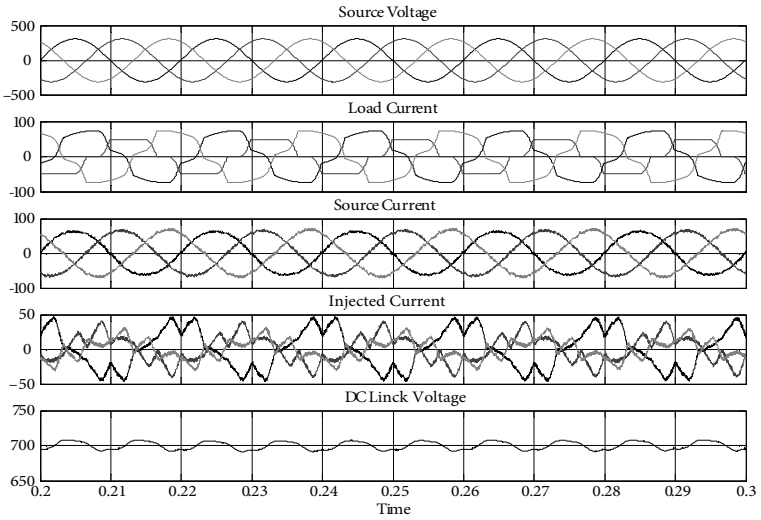

Figure 16. Simulation results of the fourth case for balancing the grid current.

Table 3. The effective values of load and grid currents in each phase in case 4.

	Load current (rms)	Source current (rms)
Phase a	54.6 A	45.5 A
Phase b	38.3 A	46.2 A
Phase c	54.4 A	46.5 A

e) In the fifth case, reactive power compensation by means of an SAPF is investigated. As it was proved in section 4.3, the proposed control system is capable of compensating reactive power in steady state. To investigate this claim, a resistive-inductive load is connected to the grid. The power factor of this load is equal to 0.66.

Simulation results of this case are shown in Figure 17. It can be seen in this figure that as time passes the SAPF compensates the grid reactive current well.

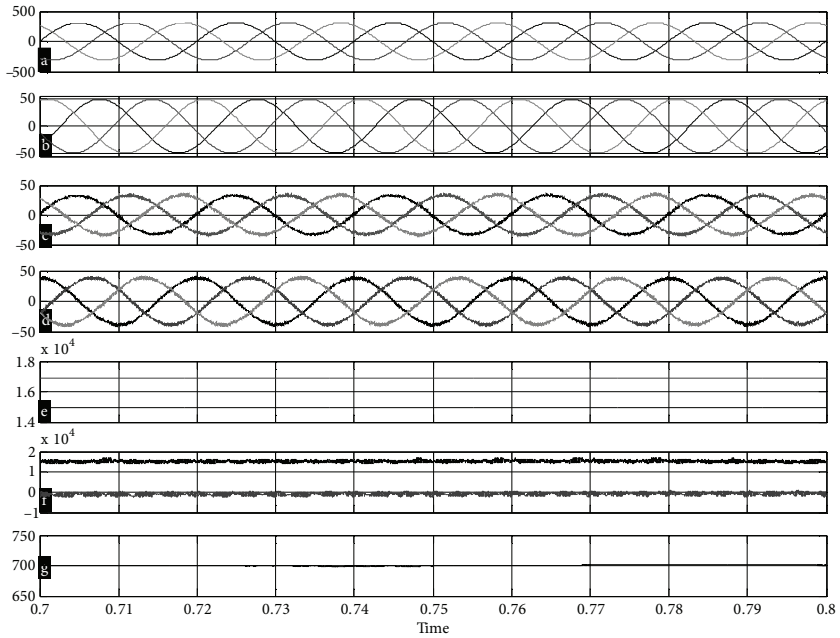

Figure 17. Simulation results of the fifth case for compensating the reactive power; a) Grid voltage, b) Load current, c) Source current, d) Current injected by the SAPF, e) Instantaneous active power and reactive power of load, f) Instantaneous active power and reactive power of the grid, g) DC link voltage.

6. Conclusions

In this paper, a new control scheme was presented for compensating power quality problems of grid current. Using an ANF, the fundamental component of the grid current was extracted and references of a control system were built based on it. The control system was designed based on proportional-resonant (PR) controller and delay limitations in digital systems. Using an indirect current control method decreased the number of required sensors to three. Therefore, two sensors are required for measuring the grid current and another sensor is needed to measure the DC link voltage. Decreasing the number of sensor reduces the cost and makes the implementation of control easier. These are two highly important advantages over other control approaches.

References

[1] Tey LH, So PL, Chu YC. Improvement of power quality using adaptive SAPF. IEEE T Power Del 2005; 20: 1558-1568.

[2] Jintakosonwit P, Fujita H, Akagi H. Control and performance of a fully-digital-controlled SAPF for installation on a power distribution system. IEEE T Power Elec 2002; 17: 132-140.

[3] Pal Y, Swarup A, Singh B. A control strategy based on UTT and ISCT for 3p4w UPQC. J World Academy of Sci Eng and Tech 2011; 75: 1284-1289.

[4] Li H, Zhou F, Wang Z, Lei W, Wu L. A novel time-domain current-detection algorithm for SAPF. IEEE T Power Sys 2005; 20: 644-651.

[5] Akagi H, Kanazawa Y, Nabae A. Instantaneous reactive power compensators comprising switching devices without energy storage components. IEEE T Ind Appl 1984; 20: 625-630.

[6] Watanabe EH, Stephan RM, Aredes M. New concepts of instantaneous active and reactive powers in electrical systems with generic load. IEEE T Power Del 1993; 8: 697-703.

[7] Fang ZP, Lai JS. Generalized instantaneous reactive power theory for three-phase power systems. IEEE T Instr Meas 1996; 45: 293-297.

[8] Asadi M, Jalilian A, Farahani HF. Compensation of unbalanced non linear load and neutral currents using stationary reference frame in SAPFs. In: IEEE 2010 14th Int Conf on Harmonics and Quality of Power; 26–29 Sept; Bergamo, Italy, New York, NY, USA: IEEE. pp. 1-5.

[9] Bhattacharya A, Chakraborty C. A shunt active power filter with enhanced performance using ANN-based predictive and adaptive controllers. IEEE T Ind Elec 2011; 58: 421-428.

[10] Bojoi RI, Griva G, Bostan V, Guerriero M, Farina F, Profumo F. Current control strategy for power conditioners using sinusoidal signal integrators in synchronous reference frame. IEEE T Power Elec 2005; 20: 1402-1412.

[11] Holmes DG, Lipo TA, McGrath BP, Kong WY. Optimized design of stationary frame three phase ac current regulators. IEEE T Power Elec 2009; 24: 2417-2426.

[12] Popescu M, Bitoleanu A, Suru V. A DSP-based implementation of the p-q theory in active power filtering under nonideal voltage conditions. IEEE T Ind Elec 2013; 9: 880-889.

[13] Miret J, Castilla M, Matas J, Guerrero JM, Vasquez JC. Selective harmonic-compensation control for single-phase active power filter with high harmonic rejection. IEEE T Ind Elec 2009; 56: 3117-3127.

[14] Tang Y, Loh PC, Wang P, Choo FH, Gao F, Blaabjerg F. Generalized design of high performance shunt active power filter with output LCL filter. IEEE T Ind Elec 2012; 59: 1443-1452.

[15] Yazdani D, Bakhshai A, Jain P. A three phase adaptive notch filter based approach to harmonic/reactive current extraction and harmonic decomposition. IEEE T Power Elec 2010; 25: 914-923.

[16] Mojiri M, Karimi-Ghartemani M, Bakhshai A. Time-domain signal analysis using adaptive notch filter. IEEE T Signal Proc 2007; 55: 85-93.

[17] Tabatabaei SH, Jalilian A, Gharaei S. Shunt active power filter control by using adaptive notch filter and proportional-integral controller. In: 27th Int power system conference; 12–14 Nov 2012; Tehran, Iran.

[18] Rahmani S, Al-Haddad K, Fnaiech F. A model reference generating an optimal dc bus voltage level for a three-phase shunt active power filter. In: IEEE 2004 11th Int Conf on Harmonics and Quality of Power; 12–15 Sept 2004; Lake Placid, New York, USA: IEEE. pp. 22-27.

[19] Ogata K. Modern Control Engineering. 5th Ed. New Jersey, USA: Prentice Hall, 2010.

[20] Bhattacharya A, Chakraborty C. A shunt active power filter with enhanced performance using ANN-based predictive and adaptive controllers. IEEE T Ind Elec 2011; 58: 421-428.

[21] Akagi H, Watanabe EH, Aredes M. Instantaneous Power Theory and Application to Power Conditioner. New York, NY, USA: Wiley-IEEE Press, 2007.